ISSN 0280–5316
ISRN LUTFD2/TFRT--5593--SE

Effects of Friction on the Furuta Pendulum

Joakim Svensson

Department of Automatic Control
Lund Institute of Technology
February 1998

Department of Automatic Control
Lund Institute of Technology
Box 118
S-221 00 Lund Sweden

Document name
Master Thesis

Date of issue
January 1998

Document Number
ISRN LUTFD2/TFRT--5593--SE

Author(s)
Joakim Svensson

Supervisor
Karl Johan Åström

Sponsoring organisation

Title and subtitle
Effects of friction on the Furuta pendulum

Abstract

This thesis investigate the frictional effects on the inverted pendulum. Because of friction, limit cycles arise when controling the pendulum in the upright position. Linear state feedback was used to control the pendulum. The control loop was improved by adding friction compensation to it. Three different friction models are tested as friction compensation, two static and one dynamic.

A mathematical model over the pendulum was made so simulations could be done. The friction models acted as friction instead of friction compensation in the simulations. When the behavior of the real pendulum without friction compensation and the simulation matched, the friction model was transfered to the real pendulum. There it work as friction compensation. It is also investigated what kind of linear state feedback that gives limit cycles.

Key words
Inverted Pendulum, Friction, Limit Cycles, Friction Compensation, LuGre Model

Classification system and/or index terms (if any)

Supplementary bibliographical information

ISSN and key title
0280–5316

ISBN

Language
English

Number of pages
24

Recipient's notes

Security classification

Contents

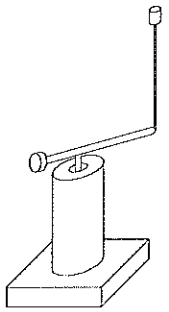

Figure 1 A figure of the inverted pendulum.

1. Introduction

This thesis is about friction on a inverted pendulum and how to compensate for it. There are several different models that describes how friction work. In this thesis three of them are considered. Friction is a very complicated, nonlinear phenomena if you want to describe it accurately. The models are all in some degree rough simplifications of the real process.

The different friction models will be tested on a inverted pendulum. The pendulum is used because when you try to control it with a linear feedback limit cycles appears. These limit cycles arise only because of friction. In Figure 1 a schematic picture over the inverted pendulum is shown. An arm is mounted to a center pillar and a pendulum is attached to the arm. Both the arm and the pendulum can be rotated. The acceleration of the arm is possible to control. It is possible to measure the position of the arm, the angle the pendulum is deflected from standing upright and the velocity of the angle. To get the velocity of the position a observer was used. The inverted pendulum is also called Furuta pendulum after K. Furuta. He was the first who developed the inverted pendulum in the form it has in this thesis.

Friction occur in two places. These are where the pendulum is attached to the arm and where the arm is mounted to the pillar. It is assumed the friction in the first place is much smaller than the second. Therefore the friction where the pendulum is attached will be neglected. When the friction models are introduced in the control algorithm, one can measure how much the behavior of the pendulum is improved. It is then possible to compare the different models and see which gives the best result.

To find suitable parameters for the friction models a mathematical model of the Furuta pendulum is made. In the model the different friction models are tested. When the mathematical model and the behavior of the real pendulum match the friction model is transfered to the real process. There it will work as friction compensation.

In this thesis it is also considered if there always will be limit cycles. Depending on which states, i.e the angle, the velocity of the angle, the position and the velocity of the position, you use as a feedback and what parameters you choose the pendulum behaves different.

The outline for the rest of the rapport is presented below. In section 2 some aspects of friction is described. Then in section 3 is the mathematical model derived and the control law that will be used. If limit cycles always occur are considered in section 4. In section 5 the behavior of the real pendulum without friction compensation is shown. In section 6 are the simulations. The result on the real pendulum with the different friction models are presented in section 7. At last in section 8 are some conclusions.

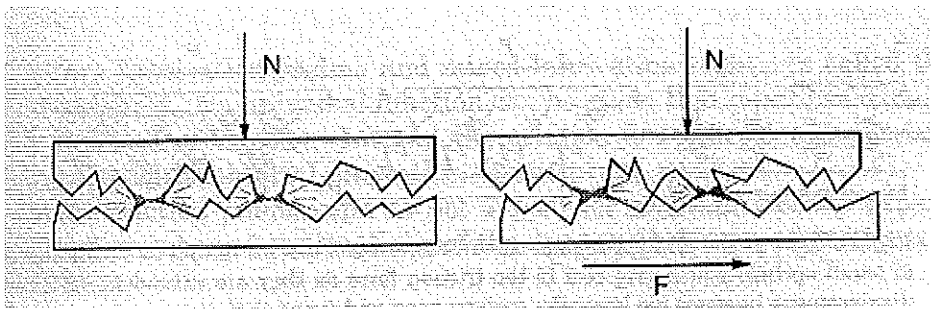

Figure 2 The microscopical contact between two surfaces. The contact takes place at a number of asperities which deform under normal and tangential loads.

2. Friction and friction models

In this section there will be a short description on how friction occurs and some friction models will be described. This section is mainly based on [1].

2.1 Friction

Friction occurs between all surfaces that are in contact with other surfaces. To understand the mechanism behind friction one has to consider what happens on a microscopical scale when two surfaces are in contact. All surfaces are rough and they are often covered with some lubricant. The actual contact takes place in a number of asperities, which are spread all over the surface. See Figure 2 a). When a tangential force is applied shearing will occur. This results in both elastic and plastic deformations. See Figure 2 b). When motion between the surfaces occur more of the lubricant will be brought into the interface.

You can roughly divide the friction mechanism, from rest to motion, into four regions of behavior, so called lubrication regimes. In Figure 3 a relation between friction force and relative velocity is shown. The lubrication regimes are also shown in the figure.

The first region is called the the *sticking regime* where the velocity between the surfaces are zero. A good mental picture of the behavior is shown in Figure 4. The contact can be viewed as formed by a number of springs. As a force is applied the springs will extend which results in the friction force. If the force becomes too large the springs will break and sliding occur.

The second regime is called *the boundary lubrication regime*. In this regime motion occurs between the surfaces but there are hardly any lubrication in the interface. The friction force is due to the shearing resistance of the asperity contacts. Normally the surfaces are covered with oxide or other compounds. The shearing resistance of these are much lower than for the metal. This makes the friction force decrease with velocity.

In *the mixed lubrication regime* the speed is increased and more lubrication brought in. This makes the separation of the surfaces larger. The friction force is partially due to the lubricant and its viscosity and partially due to asperity contacts.

In *the full fluid lubrication regime* the surfaces are completely separated by the lubricant. The friction force depends only on the hydrodynamics of the lubricant. The behavior in this regime is almost linear and is called viscous friction.

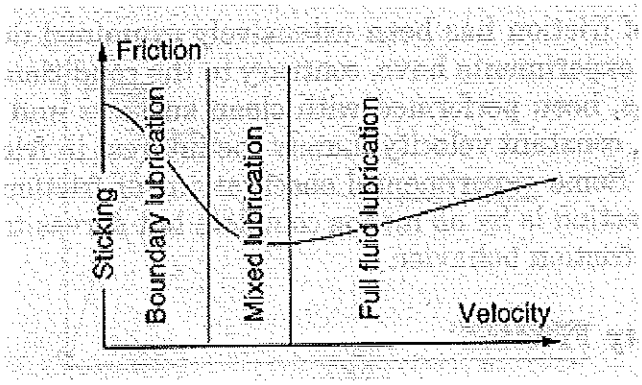

Figure 3 The Stribeck relation show a typical relation between velocity and friction force. The relation can be divided into four so called lubrication regimes. The different regions are due to the velocity dependent causes of friction.

Naturally, dynamics are involved in all the mechanisms above and therefore the complete behavior of friction is very complicated.

2.2 Friction models

There are several different friction models but they can all be divided into two categories, static- and dynamic models. In this thesis three different models will be considered, two static (Coulomb friction and Coulomb friction with stiction) and one dynamic (The LuGre model).

Coulomb friction This is the most simple friction model and the main idea is that friction opposes motion and that the friction force is independent of velocity and contact area. It can be described as

$$F = F_c sgn(v)$$

See Figure 5 a). Note that the model is not defined when the velocity is zero. To get a smoother transition from the two states, F_c and $-F_c$, another Coulomb friction model will be used. It can be described by

$$F = \begin{cases} F_C & if\ v \leq -\epsilon \\ -F_C * \frac{v}{\epsilon} & if\ |v| < \epsilon \\ -F_C & if\ v \geq \epsilon \end{cases} \quad (1)$$

where ϵ is a small number. Figure 5 b) shows the friction force as a function of velocity.

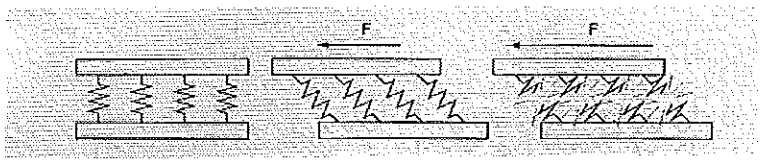

Figure 4 In the sticking regime the friction contact can be viewed as consisting of small springs which give rise to the friction force as they are extended. If the displacement becomes too large the springs snap and sliding occur.

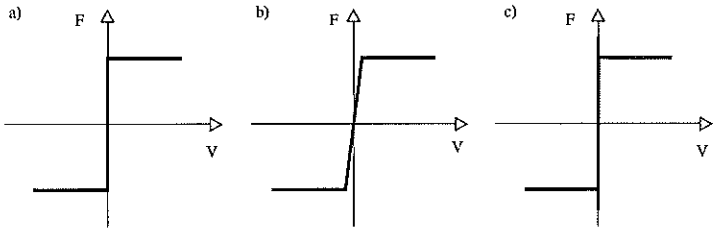

Figure 5 Examples of static friction models. The friction force is given by a static function. Figure a) shows ordinary Coulomb friction and Figure b) shows the Coulomb friction model that is used in this thesis. Coulomb friction plus stiction is shown in Figure c).

Coulomb friction with stiction Friction force when the object is at rest is included in this model. This is called stiction. Stiction is short for static friction. When the object moves it's affected by Coulomb friction. The friction model is described as

$$F = \begin{cases} F_C sgn(v) & if\ v \neq 0 \\ F_e & if\ v = 0\ and\ |F_e| \leq F_s \\ F_S sgn(F_e) & otherwise \end{cases} \tag{2}$$

where F_e is the external force and F_s denotes the stiction friction force. Figure 5 b) shows the friction force as a function of velocity.

The LuGre model This friction model is dynamic and was introduced by Canudas de Wit *et al.* Friction occurs between two surfaces in contact. Since the surfaces always are irregular the contact will take place at a number of asperities. These can be modeled as elastic bristles. In the LuGre model all bristles are replaced by a single one. The state z is the deflection of the bristle. The model consist of a first-order differential equation, an equation for the friction force and one equation that describes how the average deflection depends on the relative velocity between the moving surfaces. The model is described by

$$\begin{cases} \frac{dz}{dt} = v - \frac{|v|}{g(v)}z \\ \\ g(v) = \frac{1}{\sigma_0}(F_c + (F_s - F_c)e^{-(v/v_s)^2}) \\ \\ F = \sigma_0 z + \sigma_1 \frac{dz}{dt} + F_v v \end{cases} \tag{3}$$

Where σ_0 denotes the stiffness of the material and σ_1 is a damping coefficient. F_c, F_s and F_v denotes the friction forces for the Coulomb-, stiction- and viscous friction. The parameter v_s is the Stribeck velocity and affects the location of the minimum of the Stribeck curve, see Figure 3

3. The Inverted Pendulum

The inverted pendulum is an unstable process, but it's still fairly easy to build and to model. In this thesis a pendulum built at the Department of Automatic Control at Lund Institute of Technology, Sweden, will be used.

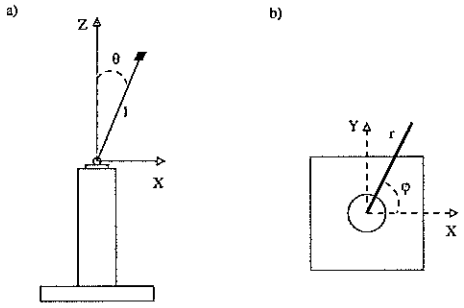

Figure 6 Views of the pendulum from the coordinate systems. Figure a) shows the pendulum from the side and Figure b) from above.

The inverted pendulum consist of an arm, a pendulum and a center pillar (See figure 6). The arm can be rotated in the horizontal plane and the pendulum that is attached to the arm can be rotated in the vertical plane. At the end of the pendulum a small is mass attached.

3.1 Mathematical Model

In this section a mathematical model of the inverted pendulum will be derived. Notice that friction and damping is neglected. The derivation is based [2]. A schematic diagram of the Furuta pendulum is shown in Figure 6.

Introduce a coordinate system with the x- and y-axes in the horizontal plane and a vertical z-axis. Let the arm which carries the pivot be of length r and let its angle with the x-axis be φ. The length of the pendulum is denoted l and let the angle with the z-axis be θ. The mass at the end of the pendulum has the coordinates:

$$\begin{aligned} x_{cm} &= r\cos\varphi - \ell\sin\theta\sin\varphi \\ y_{cm} &= r\sin\varphi + \ell\sin\theta\cos\varphi \\ z_{cm} &= \ell\cos\theta \end{aligned}$$

Taking derivatives we get

$$\begin{aligned} \dot{x}_{cm} &= -r\dot{\varphi}\sin\varphi - \ell\dot{\varphi}\cos\varphi\sin\theta - \ell\dot{\theta}\sin\varphi\cos\theta \\ \dot{y}_{cm} &= r\dot{\varphi}\cos\varphi - \ell\dot{\varphi}\sin\varphi\sin\theta + \ell\dot{\theta}\cos\varphi\cos\theta \\ \dot{y}_{cm} &= -\ell\dot{\theta}\sin\theta \end{aligned}$$

The velocity for the small mass is thus

$$v^2 = \sqrt{\dot{x}^2 + \dot{y}^2 + \dot{z}^2} = r^2\dot{\varphi}^2 + \ell^2\dot{\varphi}^2\sin^2\theta + 2r\ell\dot{\varphi}\dot{\theta}\cos\theta + \ell^2\dot{\theta}^2$$

The kinetic energy T of the whole inverted pendulum is thus given by

$$\begin{aligned} 2T &= Mv^2 + J\dot{\varphi}^2 + J_p\dot{\theta}^2 + J^*\dot{\varphi}^2 \\ &= Mv^2 + J\dot{\varphi}^2 + J_p\dot{\theta}^2 + (mr^2 + J_p\sin^2\theta)\dot{\varphi}^2 \\ &= (J + Mr^2 + mr^2 + (Jp + M\ell^2)\sin^2\theta)\dot{\varphi}^2 \\ &+ Mr\ell\dot{\varphi}\dot{\theta}\cos\theta + (J_p + M\ell^2)\dot{\theta}^2 \end{aligned}$$

Where M is the mass of the weight on the end of the pendulum, J is the moment of inertia for the arm, J_p is the moment of inertia for the pendulum, seen from the pivot and m it's mass. J^* is the moment of inertia for the pendulum seen from the center of rotation. J^* is calculated in appendix A. The potential energy is

$$V = g\ell(M + m/2)\cos\theta$$

The Lagrangian is $L = T - V$. Its partial derivatives are given by

$$\begin{aligned}
\frac{\partial L}{\partial \theta} =& - Mr\ell\dot{\varphi}\dot{\theta}\sin\theta + (J_p + M\ell^2)\dot{\varphi}^2\sin\theta\cos\theta \\
&+ g\ell(M + m/2)\sin\theta \\
\frac{\partial L}{\partial \dot{\theta}} =& (J_p + M\ell^2)\dot{\theta} + Mr\ell\dot{\varphi}\cos\theta \\
\frac{\partial L}{\partial \varphi} =& 0 \\
\frac{\partial L}{\partial \dot{\varphi}} =& Mr\ell\dot{\theta}\cos\theta + (J + Mr^2 + mr^2 + (J_p + M\ell^2)\sin^2\theta)\dot{\varphi}
\end{aligned}$$

Let u be the external forces. Euler-Lagrange's equations states that

$$\begin{aligned}
\frac{d}{dt}\left(\frac{\partial L}{\partial \dot{\theta}}\right) - \frac{\partial L}{\partial \theta} &= 0 \\
\frac{d}{dt}\left(\frac{\partial L}{\partial \dot{\varphi}}\right) - \frac{\partial L}{\partial \varphi} &= u
\end{aligned}$$

and this gives the following equations of motion

$$\begin{aligned}
&(J_p + M\ell^2)(\ddot{\theta} - \dot{\varphi}^2\sin\theta\cos\theta) \\
&\quad + Mr\ell\ddot{\varphi}\cos\theta - g\ell(M + m/2)\sin\theta = 0 \\
&Mr\ell\ddot{\theta}\cos\theta - mr\ell\dot{\theta}^2\sin\theta + 2(J_p + m\ell^2)\dot{\theta}\dot{\varphi}\sin\theta\cos\theta \\
&\quad + (J + mr^2 + (J_p + m\ell^2)\sin^2\theta)\ddot{\varphi} = u.
\end{aligned}$$

Introducing

$$\begin{aligned}
\alpha &= J_p + M\ell^2 & \beta &= J + Mr^2 + mr^2 \\
\gamma &= Mrl & \epsilon &= lg(M + m/2)
\end{aligned}$$

the equations of motion can be written as

$$\begin{aligned}
&\alpha\frac{d^2\theta}{dt^2} - \alpha\left(\frac{d\varphi}{dt}\right)^2\sin\theta\cos\theta + \gamma\frac{d^2\varphi}{dt^2}\cos\theta \\
&\qquad - \epsilon\sin\theta = 0 \\
&\gamma\frac{d^2\theta}{dt^2}\cos\theta - \gamma\left(\frac{d\theta}{dt}\right)^2\sin\theta) + 2\alpha\frac{d\theta}{dt}\frac{d\varphi}{dt}\sin\theta\cos\theta \\
&\qquad + (\beta + \alpha\sin^2\theta)\frac{d^2\varphi}{dt^2} = u
\end{aligned} \tag{4}$$

This is the model that will be used for simulations in section 6.

3.2 The control law

To control the inverted pendulum a linear state feedback will be used because it's simple and we can place the poles where we want to. The control law is:

$$u = Lx \tag{5}$$

where

$$L = \begin{bmatrix} l_1 & l_2 & l_3 & l_4 \end{bmatrix}$$

To be able to use the control law we must linearize the model described by equation 4. Introduce the state vector

$$x = \begin{bmatrix} \theta \\ \dot{\theta} \\ \varphi \\ \dot{\varphi} \end{bmatrix}$$

and linearize around $x = \begin{bmatrix} 0 & 0 & 0 & 0 \end{bmatrix}^T$, i.e. the upright position. This gives the system:

$$\frac{dx}{dt} = \begin{bmatrix} 0 & 1 & 0 & 0 \\ \frac{\beta\epsilon}{\alpha\beta-\gamma^2} & 0 & 0 & 0 \\ 0 & 0 & 0 & 1 \\ \frac{-\gamma\epsilon}{\alpha\beta-\gamma^2} & 0 & 0 & 0 \end{bmatrix} x + \begin{bmatrix} 0 \\ \frac{-\gamma}{\alpha\beta-\gamma^2} \\ 0 \\ \frac{\alpha}{\alpha\beta-\gamma^2} \end{bmatrix} u \tag{6}$$

If we insert the control law 5 into the system 6 and examine where the poles are we get:

$$s^4 + \frac{-\alpha l_2 + \gamma l_4}{\alpha\beta - \gamma^2}s^3 + \frac{-\beta\epsilon + \alpha l_3 - \gamma l_1}{\alpha\beta - \gamma^2}s^2 + \frac{\epsilon l_4}{\alpha\beta - \gamma^2}s + \frac{\epsilon l_3}{\alpha\beta - \gamma^2}$$

We want to place the poles in:

$$(s^2 + 2\zeta_1\omega_1 + \omega_1^2)(s^2 + 2\zeta_2\omega_2 + \omega_2^2)$$

We determine L in equation 5 by identifying the coefficients of the same powers of equal degree in the two expressions above. The result is

$$\begin{aligned} l_1 &= \frac{\epsilon\beta}{\gamma} + \frac{\alpha\beta - \gamma^2}{\gamma}\left(\frac{\alpha}{\epsilon}(\omega_1^2\omega_2^2) + \omega_1^2 + \omega_2^2 + 4\zeta_1\zeta_2\omega_1\omega_2\right) \\ l_2 &= \frac{\alpha\beta - \gamma^2}{\gamma}\left(\frac{\alpha}{\epsilon}(2\zeta_1\omega_1\omega_2^2 + 2\zeta_2\omega_1^2\omega_2) + 2\zeta_1\omega_1 + 2\zeta_2\omega_2\right) \\ l_3 &= \frac{\alpha\beta - \gamma^2}{\epsilon}(\omega_1^2\omega_2^2) \\ l_4 &= \frac{\alpha\beta - \gamma^2}{\epsilon}(2\zeta_1\omega_1\omega_2^2 + 2\zeta_2\omega_1^2\omega_2) \end{aligned} \tag{7}$$

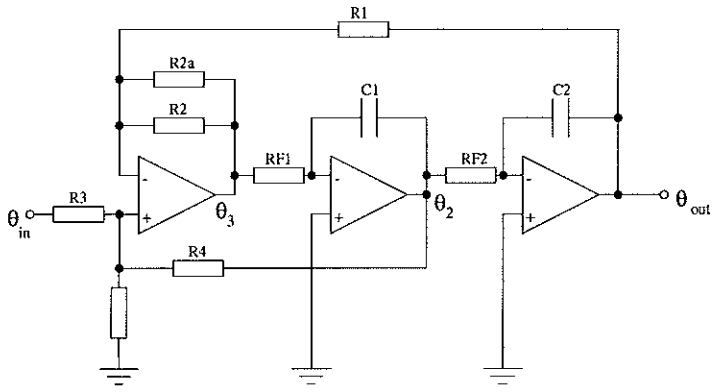

Figure 7 The low-pass filter that were made for noise reduction.

3.3 The real Furuta pendulum

In the real Furuta pendulum it is possible to measure the angles θ and φ. When measuring the signals it was found that the θ-signal was very noisy but the φ-signal was quite good. Because of this a linear observer was used to estimate $\dot{\varphi}$. To get a better θ-signal a low-pass filter was built, see Figure 7. θ_{out} is the low-passed signal. The filter can be used to estimate $\dot{\theta}$. This is shown by investigate the relation between θ_{out} and θ_2 in Figure 7.

$$\frac{\theta_2}{R_{F2}} = -\frac{\theta_{out}}{\frac{1}{C_2 s}}$$

Solving for θ_2 gives

$$\theta_2 = -R_{F2}C_2 s\theta_{out} = -R_{F2}C_2\dot{\theta}_{out}$$

One advantage with using filters is that the θ_2-signal is bandpass filtered. This is showed in appendix B where the whole filter design is done.

In order to get the model described in equation 4 as correct as possible we must determine some physical properties of the pendulum. We have to determine L, r, M, J, J_p and m. This is done in appendix C. The result is

$$L = 0.413\ m \qquad r = 0.235\ m$$
$$M = 0.01\ kg \qquad J = 0.05\ kgm^2$$
$$J_p = 0.0009\ kgm^2 \qquad m = 0.02\ Kg$$

4. Limit cycles

When trying to control the pendulum in the upright position the friction force makes the pendulum oscillate around the unstable equilibrium point. This is called limit cycles. A mathematical method to investigate if limit cycles appear is the describing function method. It can be described in the following way. You feedback your system through the nonlinearity that causes limit cycles. Initially you feed the nonlinearity with a sinus signal with amplitude C. If the amplitude of the signal is equal to C when the signal comes back, after going through the nonlinearity and the system, there probably are limit cycles. In

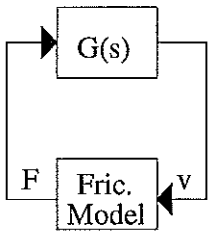

Figure 8 Feedback for limit cycles

our case the friction model is the nonlinearity, see Figure 8. The describing function method that states that limit cycles occur if

$$G(s) = -\frac{1}{Y_f(C)}$$

where $Y_f(C)$ is the describing function for the nonlinearity and C is the amplitude of the initial sinus signal. Let the friction force be Coulomb friction, i.e.

$$F = F_c sgn(\dot{\varphi})$$

If $F_c = 1.0$ the describing function will be given by

$$Y_f(C) = \frac{4}{\pi\ C}$$

From the equation above we see that $-\frac{1}{Y_f(C)}$ is the negative real axis. If $G(s)$ crosses this axis there will be limit cycles. Now we want to determine $G(s)$. Since the friction force F depends of velocity $\dot{\varphi}$ we want to have the system in the following form

$$\dot{\varphi} = G(s)F$$

To get $G(s)$ we rewrite the linearized system. From equation 6 we had that

$$\begin{aligned} \ddot{\theta} &= \frac{\beta\epsilon}{\zeta}\theta - \frac{\gamma}{\zeta}u \\ \frac{d\dot{\varphi}}{dt} &= -\frac{\gamma\epsilon}{\zeta} + \frac{\alpha}{\zeta}u \end{aligned} \tag{8}$$

where

$$\zeta = \alpha\beta - \gamma^2$$

$G(s)$ will depend on how we choose the control signal u.

4.1 Feedback from θ, $\dot{\theta}$, φ and $\dot{\varphi}$

We add friction to the control law , i.e. $u = l_1\theta + l_2\dot{\theta} + l_3\varphi + l_4\dot{\varphi} + F$, where F is the Coulomb friction force. Solving for $\dot{\varphi}$ in equation 8 gives

$$\dot{\varphi} = G(s)F = \frac{s * (\alpha\ s^2 - \epsilon)}{\zeta s^4 + (\gamma l_2 - \alpha l_4)s^3 + (\gamma l_1 - \alpha l_3 - \epsilon\beta)s * 2 + \epsilon l_4 s + \epsilon l_3} F$$

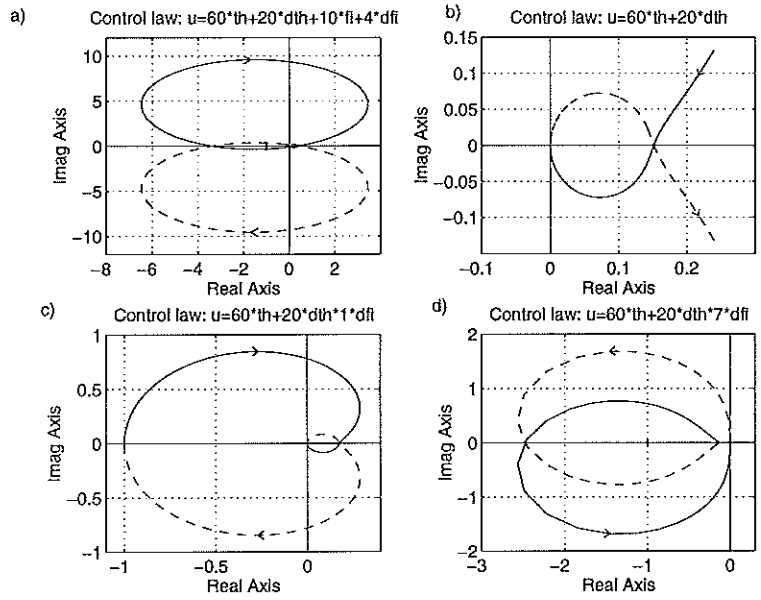

Figure 9 Nyquist plots for different feedback. Figure a) shows when the feedback $u = 60*\theta+20*\dot{\theta}+10*\varphi+4*\dot{\varphi}$ is used. In Figure b) is the feedback $u = 60*\theta+20*\dot{\theta}$ and in Figure c) and d) $u = 60*\theta+20*\dot{\theta}+\dot{\varphi}$ respectively $u = 60*\theta+20*\dot{\theta}+7*\dot{\varphi}$.

A Nyquist plot is shown in Figure 9 a). The parameters l_1, l_2, l_3 and l_4 is chosen to 60, 20, 10 respectively 4. The plot crosses the negative real axis and this predicts limit cycles. But will this occur for every choose of l_1, l_2, l_3 and l_4? As shown below this is not true for example when $l_3 = 0$ and $l_4 = 0$. Will there always be limit cycles for the control law 5 with the coefficient as equation 7? To be able to determine this we must investigate where the imaginary part of $G(s)$ is zero and see if this gives that the real part is less than zero. Inserting $s = \omega i$ in $G(s)$ gives

$$G(\omega i) = \frac{\omega i * (-\alpha\omega^2 - \epsilon)}{\zeta\omega^4 - (\gamma l_2 - \alpha l_4)\omega^3 * i - (\gamma l_1 - \alpha l_3 - \epsilon\beta)\omega^2 + \epsilon l_4 \omega i + \epsilon l_3}$$

The imaginary part of $G(\omega i)$ is zero when

$$\omega_1 = \frac{1}{2}\sqrt{-\frac{-2\gamma l_1 + 2\alpha l_3 + 2\epsilon\beta - 2K}{s}}$$

$$\omega_2 = -\frac{1}{2}\sqrt{-\frac{-2\gamma l_1 + 2\alpha l_3 + 2\epsilon\beta - 2K}{s}}$$

$$\omega_3 = \frac{1}{2}\sqrt{-\frac{-2\gamma l_1 + 2\alpha l_3 + 2\epsilon\beta + 2K}{s}}$$

$$\omega_4 = -\frac{1}{2}\sqrt{-\frac{-2\gamma l_1 + 2\alpha l_3 + 2\epsilon\beta + 2K}{s}}$$

where

$$K = \sqrt{\gamma^2 l_1^2 - 2\gamma\alpha l1 l3 - 2\gamma\epsilon\beta l1 + \alpha^2 l_3^2 + 2\alpha\epsilon\beta l_3 + \epsilon^2\beta^2 - 4\zeta\epsilon l_3}$$

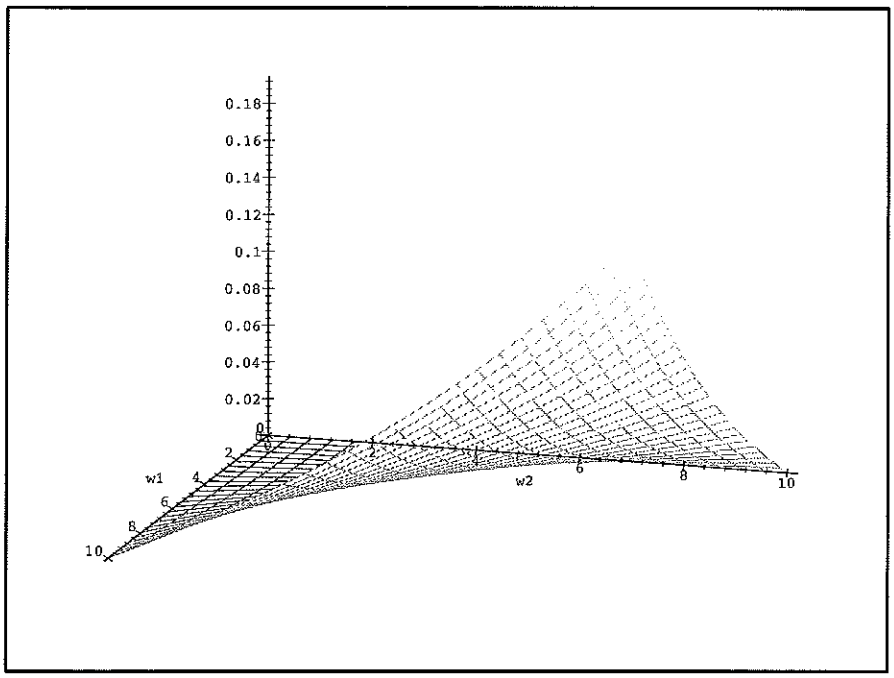

Figure 10 The figure shows that there will always be limit cycles when using the control law found in section 3.2.

The real part of $G(\omega i)$ is

$$Re(G(\omega i)) = \frac{-\omega^2(\alpha\omega^2 + e)((\alpha l_4 - \gamma l_2)\omega^2 + \epsilon l_4)}{(\zeta\omega^4 + (\alpha l_3 - \gamma l_1 + \epsilon\beta)\omega^2 + \epsilon l_3)^2 + ((\alpha l_4 - \gamma l_2)\omega^3 + \epsilon l4\omega)^2}$$

The denominator is always greater than zero if $\omega > 0$ and in the numerator is $-\omega^2(\alpha\omega^2 + \epsilon)$ always less than zero if $\omega > 0$. So we want to determine if $(\alpha l_4 - \gamma l_2)\omega^2 + \epsilon l_4$ always are greater than zero for one of the solutions to the imaginary part of $G(\omega i)$. If this is true there will be limit cycles. There are two positive solution and inserting ω_3 from above in $(\alpha l_4 - \gamma l_2)\omega^2 + \epsilon l_4$ gives

$$-\frac{-2\gamma l_1 + 2\alpha l_3 + 2\epsilon\beta + K}{4\zeta}(\alpha l_4 - \gamma l_2) + \epsilon l_4$$

We insert in this equation the expression of l_1, l_2, l_3 and l_4 from equation 7 and numerical values of the parameters α ,β, γ, ϵ and ζ based on the values of the physical parameters found in section 3.3. We also let $\zeta_1 = 0.7$ and $\zeta_2 = 0.7$. The result is an expression with two parameters ω_1 and ω_2. Note that ω_1 and ω_2 are not the same as above, they are here parameters that determine where the poles are placed. The expression are quite messy and it is not obvious that it is always greater than zero if $\omega_1 > 0$ and $\omega_2 > 0$. A 3-D plot with $\omega_1 = 0..10$ and $\omega_2 = 0..10$ indicates that this is the case, see Figure 10. This implicates that there will always be limit cycles for the control law derived in section 3.2.

4.2 Feedback from θ and $\dot{\theta}$

It can be interesting to investigate if limit cycles occur for other kinds of feedbacks. In this case we have $u = l_1\theta + l_2\dot{\theta} + F$. Solving for $\dot{\varphi}$ in equation 8

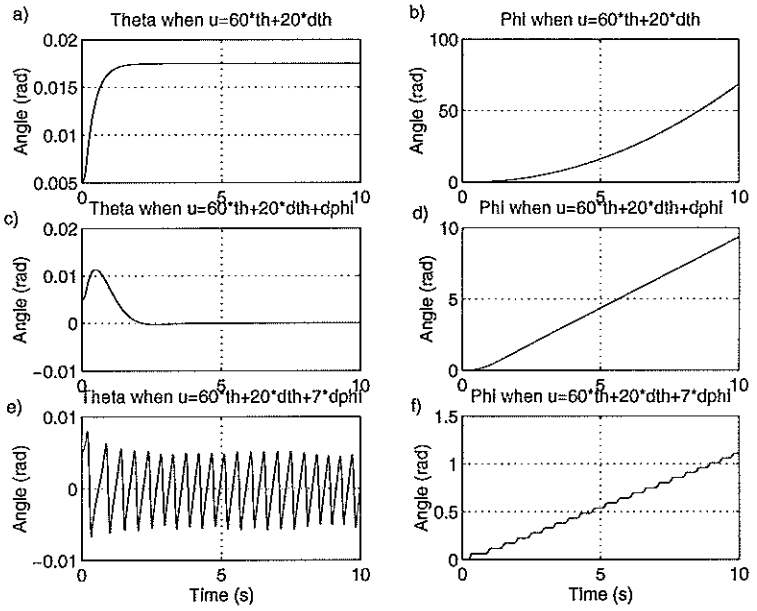

Figure 11 Simulations for different feedbacks. In Figure a) and b) is θ and φ shown when the control law $u = 60 * \theta + 20 * \dot{\theta}$ is used. In Figure c) and d) is θ and φ shown when the control law $u = 60 * \theta + 20 * \dot{\theta} + \dot{\varphi}$ is used. Finally in Figure e) and f) is θ and φ shown when the control law $u = 60 * \theta + 20 * \dot{\theta} + 7 * \dot{\varphi}$ is used.

gives

$$\dot{\varphi} = G(s)F = \frac{\alpha\zeta s^2 - \alpha\beta + \gamma^2\epsilon}{\zeta^2 s^3 + \gamma\zeta l_2 s^2 + \zeta(\gamma l_1 - \epsilon\beta)s} F \tag{9}$$

A Nyquist plot is shown i Figure 9 b). The parameters l_1 and l_2 is chosen to 60 respectively 20. The plot never crosses the negative real axis and this predicts that there are no limit cycles. In Figure 11 a,b) is a simulation. There are no limit cycles because the pendulum arm rotate in the same direction the whole time.

In order to see that no limit cycles occur independently of the physical parameters for the system and how you choose l_1 and l_2 we examine $G(s)$ in equation 9 further. Inserting $s = \omega i$ in $G(s)$ and examine the real part we get that

$$Re(G(\omega i)) = \frac{-\gamma\zeta l_2\omega(\gamma^2\epsilon - \alpha\epsilon\beta - \alpha\zeta\omega^2)}{(\gamma\zeta l_2\omega^2)^2 + (\zeta(\gamma l_1 - \epsilon\beta)\omega - \zeta^2\omega^3)^2}$$

The denominator is always real and greater than or equal to zero. In the numerator $-\gamma\zeta l_2\omega$ is less than or equal to zero and $\gamma^2\epsilon - \alpha\epsilon\beta - \alpha\zeta\omega^2 = -(\alpha\beta - \gamma^2)(\epsilon + \alpha\omega^2)$, since $\zeta = \alpha\beta - \gamma^2$. The expression $\epsilon + \alpha\omega^2$ is always greater than zero. To get the numerator greater than or equal to zero $\alpha\beta - \gamma^2$ must be greater than or equal to zero.

$$\alpha\beta - \gamma^2 = (J_p + ml^2)(J + mr^2 + m_p r^2) - m^2 r^2 l^2 =$$
$$= J_p J + mr^2 J_p + m_p r^2 J_p + ml^2 J + mm_p r^2 l^2 \geq 0$$

For the control law $u = l_1\theta + l_2\dot{\theta}$ with Coulomb friction limit cycles never occur irrespectively of physical parameters and how you choose l_1 and l_2.

4.3 Feedback from θ, $\dot{\theta}$ and $\dot{\varphi}$

Another possible feedback is $u = l_1\theta + l_2\dot{\theta} + l_3\dot{\varphi} + F$. Solving for $\dot{\varphi}$ in equation 8 gives

$$\dot{\varphi} = G(s)F = \frac{\alpha s^2 - \epsilon}{\zeta s^3 + (\gamma l_2 - \alpha l_3)s^2 + (\gamma l_1 - \epsilon\beta s + \epsilon l_3)}F \tag{10}$$

A Nyquist plot is shown i Figure 9 c). The parameters l_1 l_2 and l_3 is chosen to 60, 20 and 1. The plot never crosses the negative real axis and this predicts that there are no limit cycles.

In order to see that if there can be limit cycles depending on how you choose l_1 , l_2 and l_3 we examine equation 10 further. Inserting $s = \omega i$ in $G(s)$ and examining the imaginary part we get that

$$Im(G(\omega i)) = \frac{\omega(\alpha\omega^2 + \epsilon)(-\zeta\omega^2 + \gamma l_1 - \epsilon\beta)}{((\alpha l_3 - \gamma l_2)\omega^2 + \epsilon l_3)^2 + (-\zeta\omega^3 + (\gamma l_1 - \epsilon\beta)\omega)^2} \tag{11}$$

Equation 11 is zero when $\omega^2 = \frac{\gamma l_1 - \epsilon\beta}{\zeta}$. The real part of $G(\omega i)$ is

$$Re(G(\omega i)) = \frac{-(\alpha\omega^2 + \epsilon)((\alpha l_3 - \gamma l_2)\omega^2 + \epsilon l_3)}{((\alpha l_3 - \gamma l_2)\omega^2 + \epsilon l_3)^2 + (-\zeta\omega^3 + (\gamma l_1 - \epsilon\beta)\omega)^2}$$

The denominator is always greater than zero if $\omega > 0$. In the numerator $-(\alpha\omega^2+\epsilon)$ is less than zero if $\omega > 0$. Limit cycles occur if $(\alpha l_3 - \gamma l_2)\omega^2 + \epsilon l_3 \geq 0$ when inserting $\omega^2 = \frac{\gamma l_1 - \epsilon\beta}{\zeta}$ into the equation. Doing this gives that

$$(\alpha l_3 - \gamma l_2)\omega^2 + \epsilon l_3 = \frac{\gamma}{\zeta}(\alpha l_1 l_3 - \gamma l_1 l_2 + \epsilon\beta l_2 - \epsilon\gamma l_3)$$

This expression can be both positive and negative depending on how you choose l_1, l_2 and l_3. For example using $l_1 = 60$, $l_2 = 20$ and $l_1 = 1$ gives that the expression above has the value -9.78 if we use the physical parameters found in 3.3. This implicates that there will be no limit cycles. As we saw in Figure 9 c) the Nyquist plot never crosses the negative real axis. A simulation of the linearized model shows what happens, see Figure 11 c,d). The pendulum arm rotates in the same direction the whole time with a constant velocity. The pendulum stands still in angle slightly more than zero. There are no limit cycles.

If we instead use $l_1 = 60$, $l_2 = 20$ and $l_1 = 7$ the expression above has the value 7.04. This implicates that there will be limit cycles. By looking at a Nyquist plot, see Figure 9, we see that the curve crosses the negative real axis. A simulation of the linearized model shows what happens, see Figure 11 e,f). The pendulum arm is either still or moves in the same direction and the pendulum oscillates around the equilibrium point. There are limit cycles.

5. The real Furuta pendulum with no friction compensation

We want to see how the Furuta pendulum behaves when there are no friction compensation. That is because when simulating the model described in

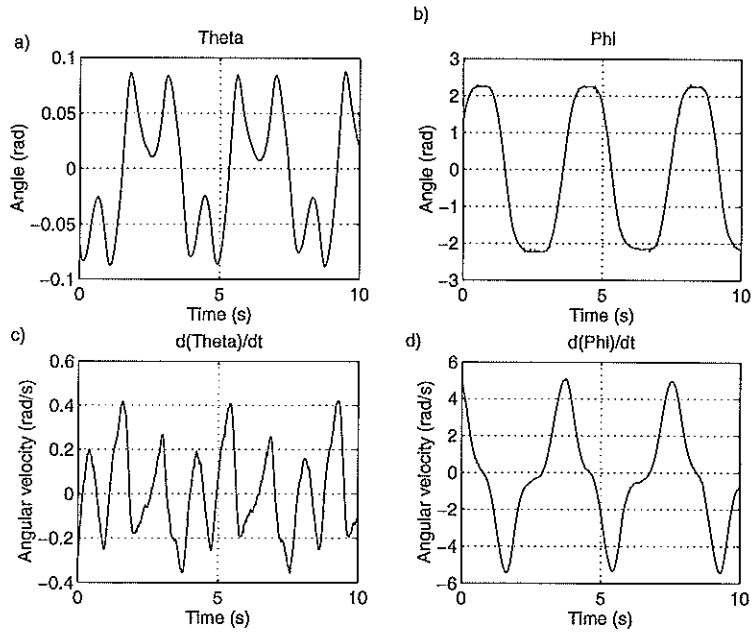

Figure 12 Result from measurement of the real pendulum. $\theta, \varphi, \dot{\theta}, \dot{\varphi}$ is plotted in Figure a), b), c) respectively d)

equation 4 with different friction models we want the simulation to behave as similar as possible to the real pendulum. Then we can take the friction model from the simulations and use it as friction compensation at the real pendulum. In Figure 12 are measurements of the four different states θ, $\dot{\theta}$, φ and $\dot{\varphi}$ plotted when controlling the real pendulum. The control law 5 was used with $\omega_1 = 3.0$ and $\omega_2 = 7.0$. The dampening coefficients ζ_1 and ζ_2 were both set to 0.7. By looking at the $\dot{\varphi}$-plot one can see that $\dot{\varphi}$ is almost never zero, so there are probably no stiction. An attempt to increase the friction and thereby also the stiction regime was made but this damaged the pendulum. The θ-plot was found to have the standard deviation 0.055 radians. For the φ-plot the standard deviation 1.49 radians. The control signal has a standard deviation of 0.72 radians.

6. Simulations

Simulation is done for the three different friction models that were described in section 2.2. Because the friction force in the real model didn't have much stiction the three models look almost the same. Therefore we only describe in detail what happens when we have Coulomb friction with stiction.

6.1 Coulomb friction with stiction

The friction model described in equation 2 is used. In our case $v = \varphi'$ and we set φ' equal to zero if $|\varphi'| \leq 0.02$. If we choose a smaller value to get less stiction the friction model starts to behave strange. It starts to oscillate very fast between the states when $\dot{\varphi}$ is small. The result is that the pendulum behaves as if there were stiction.

We simulate the model described in equation 4 with the control law as in

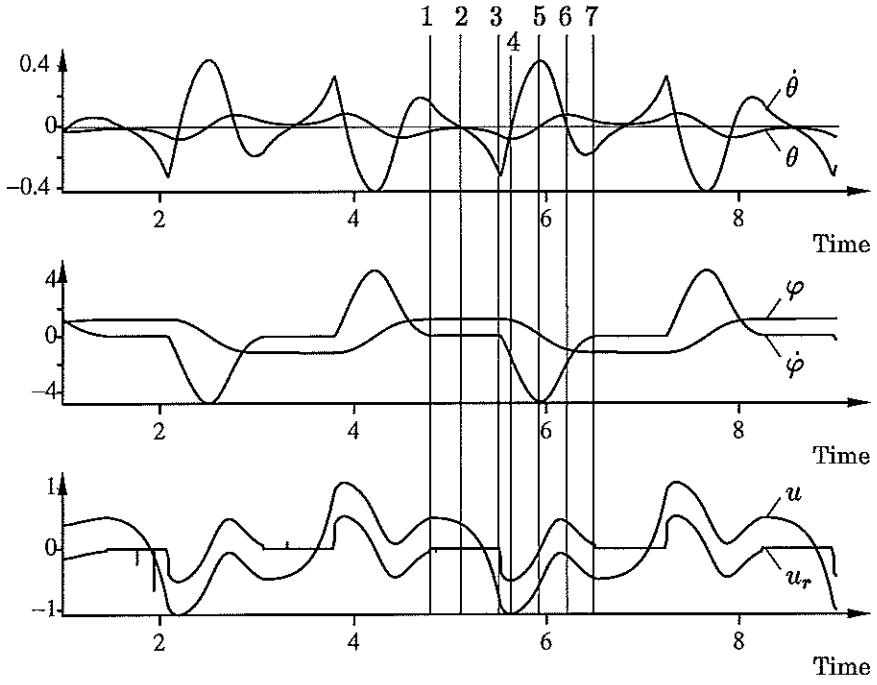

Figure 13 Pendulum with coulomb friction. In Figure a) is θ and $\dot{\theta}$ shown and in Figure b) φ and $\dot{\varphi}$. In Figure c) the control signal u and the resulting control signal $u_r = u - F$ is shown.

equation 5 with the parameter as in equation 7. We choose $\omega_1 = 3.0$, $\omega_2 = 7.0$ and $\zeta_1 = \zeta_2 = 0.7$. The arm of the pendulum is affected by the friction force described in equation 2. The result is shown in Figure 13. U_r is the resulting force i.e. $u_r = u - F$. We investigate the different sections to see what happens.

1 Stiction occurs because $\dot{\varphi} < 0.02$. Gravitation makes the pendulum deaccelerate.

2 There is still stiction, but $\dot{\theta}$ changes sign so the pendulum starts to fall.

3 The control signal has become so large that $u > F_s$ which means that stiction stops and the pendulum arm starts to move. $\dot{\varphi}$ increases and become larger than 0.02. This makes the friction force equal to F_c and the resulting control force increases very rapidly. The pendulum arm chases the pendulum so it won't fall. $\dot{\theta}$ starts to decrease.

4 $\dot{\theta}$ changes sign and the pendulum doesn't fall anymore. It's on its way to stand up.

5 The pendulum passes zenith but the speed is too large so it passes right by and starts to fall. The control signal changes sign to stop the arm and $\dot{\varphi}$ decreases and this leads to that also $\dot{\theta}$ decrease. This happens because the velocity at the top of the pendulum, i.e. where the mass is attached, is greater than velocity at the end of the pendulum arm, when $\dot{\varphi}$ decreases.

6 $\dot{\theta}$ changes sign and the pendulum starts to stand up.

7 Stiction occurs once again and we are back to where we started.

In figure 13 it is hard to compare how much alike the simulation is with the real model. Therefore we compare θ and φ for the simulation above and the

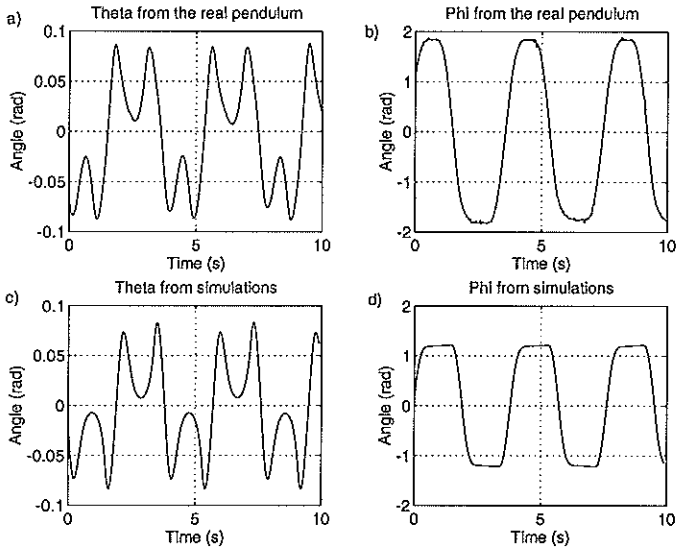

Figure 14 Comparison between the real pendulum and the simulation. In Figure a) and c) is θ shown for measurement from the real pendulum respectively from simulations. In Figure b) and d) is φ shown for measurement from the real pendulum and from simulations.

real Furuta pendulum without friction compensation when we have the same scale on the axes. See Figure 14. The simulation behaves almost exactly as the real process, except that the pendulum arm stops when stiction occurs in the simulation.

7. The real Furuta pendulum with friction compensation

The three different friction models in section 2.2 are used. The parameters for the models were chosen so that the simulation behaved as the real pendulum as much as possible.

7.1 Coulomb friction compensation

In Figure 15 a,b) is θ and φ plotted. The result is very good. The standard deviation for the θ-plot and the φ-plot is 0.044 radians respectively 0.05 radians compared to 0.055 radians and 1.49 radians with no friction compensation. This is a factor 10 better for θ and almost a factor 30 for φ. For the control law the standard deviation is 0.46 radians compared to 0.72 radians. It is natural that the standard deviation for the control signal doesn't change so must, because with no friction compensation the control law is $u = l_1\theta + l_2\dot{\theta} + l_3\varphi + l_4\dot{\varphi}$. With friction compensation we have the following control law $u = l_1\theta + l_2\dot{\theta} + l_3\varphi + l_4\dot{\varphi} + F$. The friction force F makes the standard deviation become larger.

7.2 Coulomb friction with stiction compensation

In Figure 15 c,d) is θ and φ plotted. The standard deviation for θ and φ is 0.0045 radians respectively 0.05 radians. This result is almost the same as for

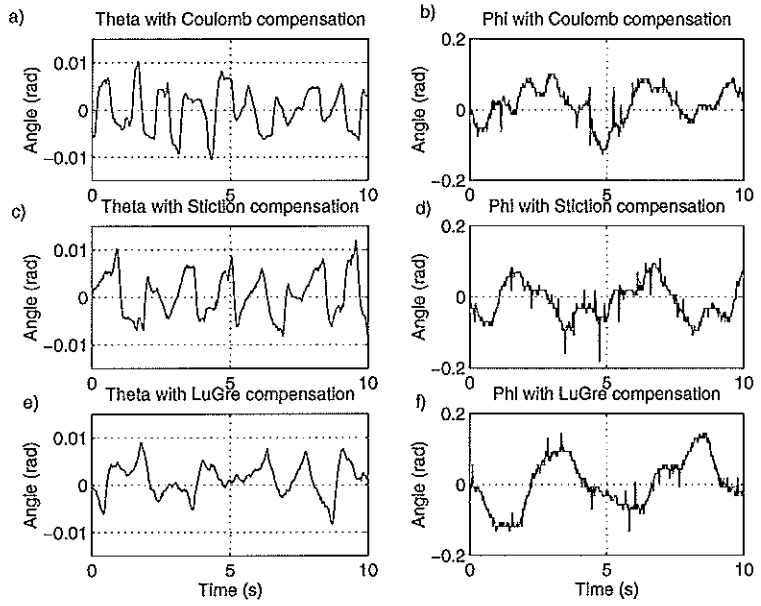

Figure 15 Result of the different friction models on the real pendulum. In Figure a) and b) is θ and φ shown when Coulomb friction compensation is used. In Figure c) and d) is θ and φ shown when stiction compensation is used. In Figure a) and b) is θ and φ shown when LuGre compensation is used.

Coulomb friction. This once again implicates that there are no stiction. The standard deviation is 0.49 radians for the control signal.

7.3 LuGre friction compensation

In Figure 15 is θ and φ and plotted. The standard deviation for θ and φ is 0.0033 radians respectively 0.07 radians compared to 0.055 radians and 1.49 radians with no friction compensation. This is almost a factor 20 better for θ and a factor 20 for φ. If you measure several times you find that the standard deviation for θ is half of what you get if you use Coulomb friction and Coulomb friction with stiction compensation. The standard deviation for φ is approximately the same for the different models. The LuGre model is probably better because it is a dynamic model so it is smoother than the other models. The standard deviation for the control signal is 0.052 radians.

When you are lucky and the different factors, that you haven't taken into account, that affects the pendulum are minimal, you can get extremely good results with the LuGre friction model. In Figure 16 is a plot when the pendulum actually stands still in the upright position. Why can the LuGre model give that much better result than the other two models? IF there are no stiction all the models should be equally good. The Coulomb friction model doesn't take the external forces into account when φ is zero. Therefore it can never make the pendulum to stand still if the friction force isn't exactly the same as the one the model predict and if there are no bias to the signals used in the feedback. The Coulomb friction with stiction take the external forces into account so it is possible to get the pendulum to stand still, but the model is static and has discontinuities which makes it difficult. The LuGre model is a dynamic model and that means that the transitions between the different states are smooth. This is probably why the LuGre model works so good.

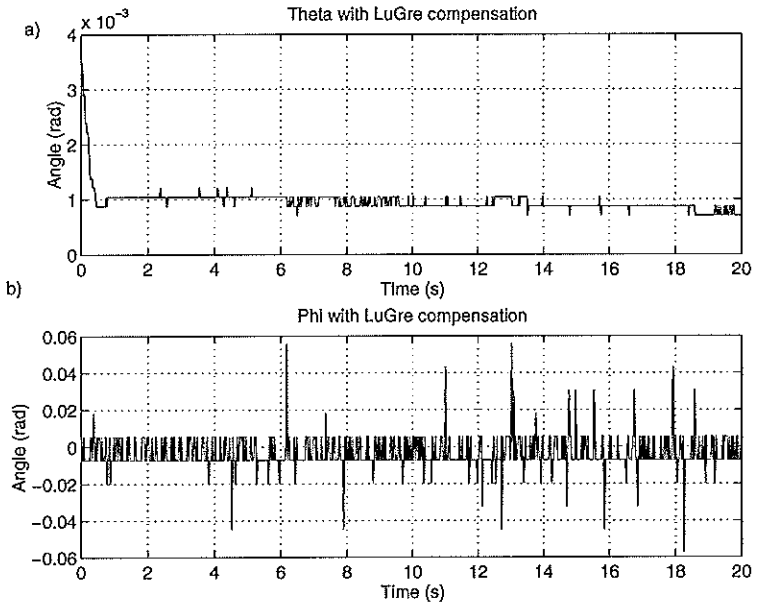

Figure 16 The pendulum stands still with LuGre friction compensation. In Figure a) is θ plotted and in Figure b) φ.

8. Conclusions

In this thesis has friction on the inverted pendulum been studied. An accurate model for the pendulum has been made, so you can simulate your friction models before you use them on the real pendulum. The pendulum has been controlled with linear feedback.

Three different friction models has been used, two static and one dynamic. The pendulum has almost no stiction. Therefore all three models give good results, but the best result is given with the dynamic model. This probably depends on that there are smooth transitions between the states in this model. It has also been showed that the pendulum behaves very different depending on what kind of feedback you use.

In this thesis has only the improvement for one set of parameters in the control law been considered. The control law was chosen to be quite slow. It would be interesting to see how friction compensation works with a faster control loop and different control strategies. The pendulum didn't have much stiction so even a simple model as the Coulomb friction model give good results. Since this model only has one parameter, F_c, it would interesting to have some kind of adaptation for this parameter.

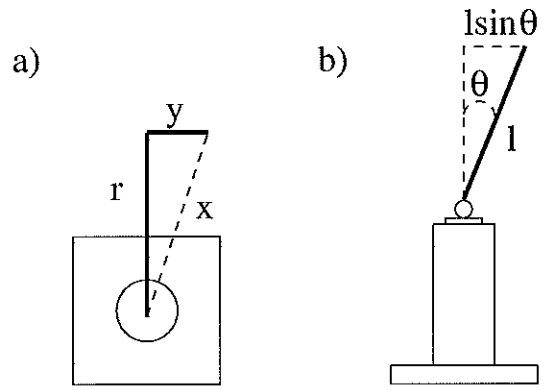

Figure 17 Figure a) shows the pendulum from above and Figure b) from the side.

A. Moment of inertia for the pendulum, seen from center of rotation

From the definition of moment of inertia we have that

$$J^* = \int x^2 dm$$

where the integral is performed over the whole body. Here is x the perpendicular distance from the axis of rotation to the small mass element dm on the pendulum. In our case is (See Figure 17) $x^2 = r^2 + y^2$ and $dm = \frac{m}{l \sin\theta} dy$. Where m is the total mass of the pendulum. This gives

$$J^* = \int_0^{l\sin\theta} (r^2 + y^2) \frac{m}{l \sin\theta} dy =$$
$$= r^2 m + \frac{ml^2}{3} \sin^2\theta$$

If we calculate the moment of inertia for the pendulum with the center of rotation at the pivot the result is

$$J_p = \frac{ml^2}{3}$$

so we can write

$$J^* = r^2 m + J_p \sin^2\theta$$

B. Filter design

From experiment it was found that the noise had frequency above $\omega \approx 15$ radians/s. A second order Bessel-filter is used, see Figure 7. The relation between θ_{out} , θ_2 and θ_3 is

$$\begin{aligned}
\theta_{out} &= -\frac{1}{R_{2F}C_2 s}\theta_2 \\
\theta_2 &= -\frac{1}{R_{1F}C_1 s}\theta_3 \\
\theta_3 &= R_6\theta_{in} + R_7\theta_2 - \frac{R_{2tot}}{R_1}\theta_{out}
\end{aligned}$$

where

$$\begin{aligned}
R_6 &= \frac{R_2 + R_1}{R_1}\frac{R_4R_Q}{R_4R_Q + R_3R_Q + R_3R_4} \\
R_7 &= \frac{R_2 + R_1}{R_1}\frac{R_3R_Q}{R_4R_Q + R_3R_Q + R_3R_4} \\
R_{2tot} &= \frac{R_2R_{2a}}{R_2 + R_{2a}}
\end{aligned}$$

This gives that

$$\begin{aligned}
\theta_{out} &= \frac{R_6}{R_{1F}R_{2F}C_1C_2s^2 + R_7R_{2F}C_2s + \frac{R_{2tot}}{R_1}}\theta_{in} \\
\theta_2 &= -\frac{R_{2F}C_2R_6}{R_{1F}R_{2F}C_1C_2s^2 + R_7R_{2F}C_2s + \frac{R_{2tot}}{R_1}}\theta_{in}
\end{aligned}$$

It is clearly seen that θ_{out} is the low-pass signal of θ_{in} and θ_2 is the derivate of the low-passed signal. It is also possible to see that θ_2 is band-pass filtered. By choosing the resistance right it is possible to get the break frequency and amplifying we wanted. This is done with a computer program.

C. Data for the pendulum

The length of the arm and the pendulum were measured to be 0.235 m respectively 0.413 m. The mass of weight at the end of the pendulum was easily measured with a scale. It was found to be 10 g. The mass of the pendulum was 20 g.

There are two ways to determine the moment of inertia for the pendulum. One mathematical and one experimental. If everything is correct they will give approximately the same result.

The mathematical method uses the definition of moment of inertia, which states that

$$J_p = \int r_i^2 * dm_i$$

where r_i is the perpendicular distance from the axis of rotation to the small mass element dm_i. The pendulums total moment of inertia is found by integrating over the whole body. Doing this gives

$$J_p = \frac{1}{3}mL^2$$

Where m is the mass of the pendulum. Inserting the values from above gives that

$$J_p = 0.0011\ kgm^2$$

The experimental method uses that for a pendulum is

$$T = 2\Pi\sqrt{\frac{J_p}{mgd}}$$

where T is the period time, J_p the moment of inertia and m the mass. The parameter d is the distance from the axis of rotation to the center of gravity on the pendulum. Solving for J_p gives

$$J_p = \frac{T^2 mgd}{4\Pi^2}$$

Experiment gives that $T = 1.12\ s$, $m = 20\ g$ and $d = 15.3\ cm$. The result is

$$J_p = 0.0009\ kgm^2$$

The mathematical and the experimental method match quite good, but the experimental is most likely to have given the most exact value.

The moment of inertia for the pendulum arm was more difficult to find because it's not possible to remove the pendulum arm from the experimental setup. It was estimated from simulations. The result was

$$J = 0.05\ Kgm^2$$

D. References

[1] H. Olsson, "Control System with Friction", PhD thesis, Department of Automatic Control, Lund Institute of Technology, Lund, Sweden, 1996.

[2] J. Eker and K. J. Åström, "A nonlinear observer for the inverted pendulum", Technical Rapport, Department of Automatic Control, Lund Institute of Technology, Lund, Sweden, 1996.

[3] K. J. Åström and B. Wittenmark, "Computer Controlled Systems — Theory and Design", Prentice-Hall, 1997.

[4] T. Glad and L. Ljung, "Reglerteknik — Grunläggande teori", Studentlitteratur, 1989.

[5] D. Cunningham and J. Stuller, "Basic Circuit Analysis", Houghton Mifflin, 1991.

[6] K. J Åström and K. Furuta, "Control Principles with Applications to Pendulums".

[7] C. F. Abelsson, "The Effect of Friction on Stabilization of an Inverted Pendulum", Master thesis, Department of Automatic Control, Lund Institute of Technology, Lund, Sweden, 1996.

[8] H. Young, "University Physics", Addison Wesley, 1992.

[9] H. Olsson, K. J Åström, C. Canudas de Wit, M. Gävert, P. Lischinsky, "Friction Models and Friction Compensation".